Interaction Between Solid Copper Jets and Powerful Electrical Current Pulses

Patrik Appelgren[1]
e-mail: patrik.appelgren@foi.se

Torgny E. Carlsson

Andreas Helte

Tomas Hurtig

Anders Larsson

Patrik Lundberg

Melker Skoglund

Lars Westerling

Swedish Defence Research Agency (FOI),
SE-164 90 Stockholm, Sweden

The interaction between a solid copper jet and an electric current pulse is studied. Copper jets that were created by a shaped-charge device were passed through an electrode configuration consisting of two aluminum plates with a separation distance of 150 mm. The electrodes were connected to a pulsed-power supply delivering a current pulse with amplitudes up to 250 kA. The current and voltages were measured, providing data on energy deposition in the jet and electrode contact region, and flash X-ray diagnostics were used to depict the jet during and after electrification. The shape of, and the velocity distributions along, the jet has been used to estimate the correlation between the jet mass flow through the electrodes and the electrical energy deposition. On average, 2.8 kJ/g was deposited in the jet and electrode region, which is sufficient to bring the jet up to the boiling point. A model based on the assumption of a homogenous current flow through the jet between the electrodes underestimates the energy deposition and the jet resistance by a factor 5 compared with the experiments, indicating a more complex current flow through the jet. The experimental results indicate the following mechanism for the enhancement of jet breakup. When electrified, the natural-formed necks in the jet are subjected to a higher current density compared with other parts of the jet. The higher current density results in a stronger heating and a stronger magnetic pinch force. Eventually, the jet material in the neck is evaporated and explodes electrically, resulting in a radial ejection of vaporized jet material. [DOI: 10.1115/1.4002568]

1 Introduction

When a high enough current is forced through a thin conductor, the conductor will be heated, melted, and eventually evaporated. If the deposition of electric energy is sufficiently fast, the conductor will explode electrically. The case is more complex if the conductor is moving so that new and unheated conductor material enters the active region where current is conducted. After the current interaction, the conductor may particulate and the fragments may transform into rings or thin disks. In this paper, the experimental results presented by Appelgren et al. [1] are analyzed further. In that paper, the disruption of the jet *after* the passage of the electrodes was studied, and it was shown that the electrification accelerated the natural fragmentation of the jet and the jet fragments were disintegrated into smoke rings with minimal penetration ability. Here, the effects of electrification of the jet *between* the electrodes are studied. The radius along the jet and velocity distribution at a specific time from initiation of an unelectrified jet from the shaped-charge device has been used in this analysis. The jet shape is calculated and the jet flow between the electrodes is correlated with the deposited electric energy in the jet. The heating, and resistance increase, of the jet is calculated using the current action integral representation and the experimentally measured current. The enhanced fragmentation of the jet due to the current passing through the jet is studied in the X-ray pictures and estimations of the instability growth were obtained.

2 Experimental Arrangements

The experimental setup has been presented in detail elsewhere [1]. A copper jet, created by using a shaped-charge device, is passed through an electrode configuration consisting of two 5 mm thick aluminum plates separated by 150 mm. The electrodes were connected to a 400 kJ pulsed-power supply (PPS), mainly consisting of a capacitor bank, delivering a current pulse with an amplitude up to 250 kA and a duration of 100 μs [2]. Current and voltage were measured yielding data on energy deposition in the jet and electrode contact region and X-ray radiography were used to depict the jet during and after electrification. Three tests are used in the analysis here, where the initial energy in the capacitor bank of the pulsed-power supply was varied. The initial energy and the times when the X-ray pictures were taken are given in Table 1.

A typical current trace from an experiment is shown in Fig. 1. The PPS was charged to 10.6 kV corresponding to 96.3 kJ. The current rise time (10–90% of peak current) was 16 μs, and the full width at half maximum (FWHM) value was 98 μs. The pulse width was 129 μs, measured from the onset of current until it drops back down to 0 kA. Figure 2 shows the jet 81 μs or 86 μs after it has made contact with electrode 2 for three different values of the capacitor bank energy (0 kJ, 39 kJ, and 96 kJ). The jet moves from left to right and the shadowed regions on the left hand side are the positions of the electrodes. The jet disruption clearly increases with energy and the disruption begins earlier.

3 Analysis of Jet Flow Between the Electrodes

3.1 Properties of an Unelectrified Jet. Prior to the electrifying experiments, the properties of an unelectrified jet were determined for the part of the jet that has a velocity above 2.1 km/s. Figure 3 shows the jet radius and jet velocity distribution at the time the tip makes contact with electrode 2 and the current begins to flow as functions of distance to the cone base of the shaped charge. With this information, it is possible to calculate the jet shape at any time before the jet starts to break up into fragments and, if a constant mass density throughout the jet is assumed, the jet mass distribution can be obtained. Figure 4 shows a position-time diagram for the jet with the positions of the electrodes indi-

[1]Present address: Division of Space and Plasma Physics, School of Electrical Engineering, Royal Institute of Technology, SE-100 44 Stockholm, Sweden.

Contributed by the Applied Mechanics of ASME for publication in the JOURNAL OF APPLIED MECHANICS. Manuscript received September 9, 2009; final manuscript received February 25, 2010; accepted manuscript posted September 16, 2010; published online November 8, 2010. Assoc. Editor: Vikram Deshpande.

Table 1 The initial energy in the PPS and the times when the X-ray photographs were taken for the three experiments used in the analysis

Initial energy in the PPS (kJ)	Electrode separation (mm)	X-ray times (μs)
0	150	31, 81, 81
39	150	36, 86, 86
96	150	36, 86, 86

cated by the horizontal lines. The jet shapes at five different times are included in the diagram, illustrating the stretching and accompanied reduction in radius. Figure 5 shows the mass as function of time of a jet passing between two electrodes with 150 mm separation distance. Line A is the mass of the part of the jet that has not made contact with electrode 1. Line B is the mass of the part of the jet that is between the two electrodes and line C is the mass of the jet that has passed electrode 2. The jet total mass is given by line D. The analysis here does not include jet elements with a velocity lower than 2.1 km/s and hence the mass included in the analysis will drop as the 2.1 km/s segment moves toward the second electrode indicated by the dashed part of line B. Figure 6 shows the jet radius at electrodes 1 and 2 are calculated using the data shown in Fig. 3. Apart from the tip fragment at electrode 2, at the first 10 μs, the jet radius at the electrodes continuously increases with time. This implies that the jet radius along the part of the jet that is between the electrodes will increase with time. Hence, the cross-sectional area of the part of the jet that is between the electrodes will increase in time despite the stretching of the jet.

3.2 Interaction Between the Jet and the Current Pulse. Figures 7–9 show the position-time diagram for the jet in the experiments together with the traces of the measured current, energy, and power. The position-time diagram is the same for both

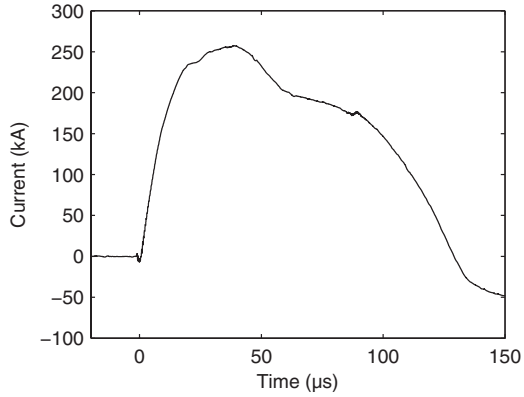

Fig. 1 The measured current pulse in the 96 kJ experiment

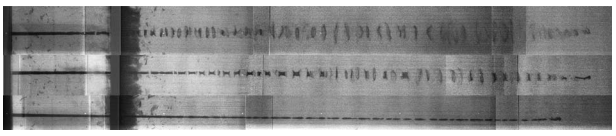

Fig. 2 X-ray pictures of jet disruption at different initial energy in the PPS. From top, 96 kJ, 39 kJ, and 0 kJ are stored in the PPS. The jet moves from left to right and the shadowed areas on the left hand side are the positions of the electrodes. The pictures are taken at 86 μs after contact is made by the tip with electrode 2, except for the lower picture taken at 81 μs after contact. The jet tip has moved a distance of 620 mm from the electrode 2 at time 86 μs.

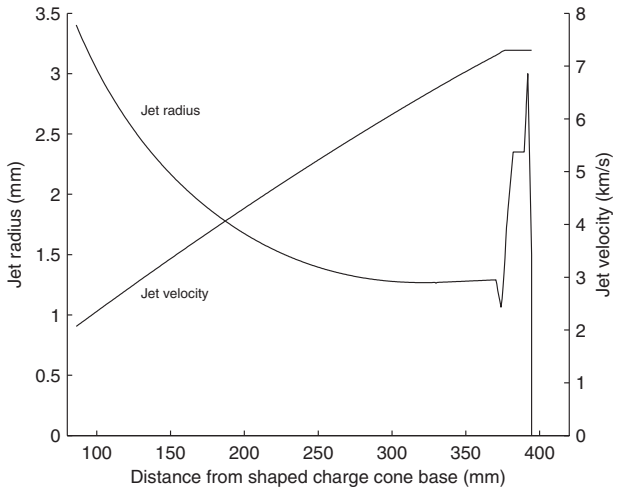

Fig. 3 The jet radius and jet velocity distribution at the time the tip makes contact with electrode 2 and the current begins to flow, as functions of distance to the cone base of the shaped charge

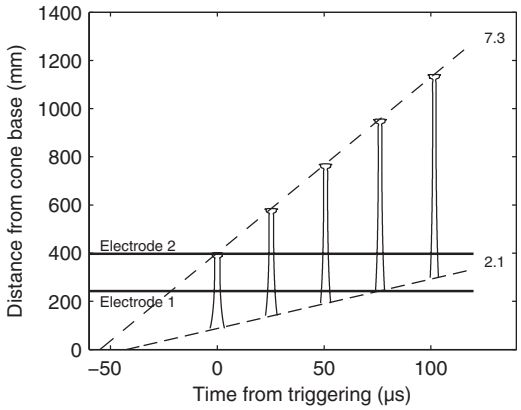

Fig. 4 Position-time diagram for the jet used in the experiments. The sloped lines indicate the jet segment velocity for the tip and rear, given by the numbers in km/s. The jet shape at five times is shown where the stretching is clearly illustrated.

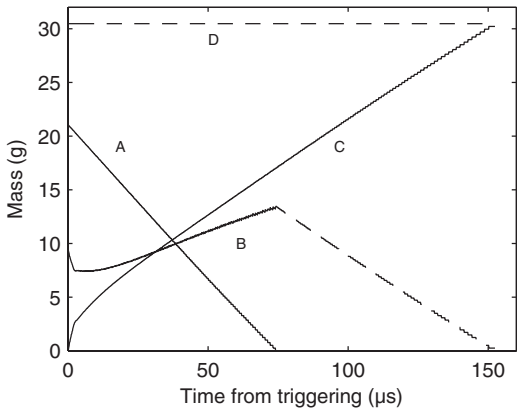

Fig. 5 Distribution of the jet mass for jet segments with an axial velocity above 2.1 km/s. The jet mass before (A), in between (B), and after (C) the electrodes summing up to the total mass indicated by line D.

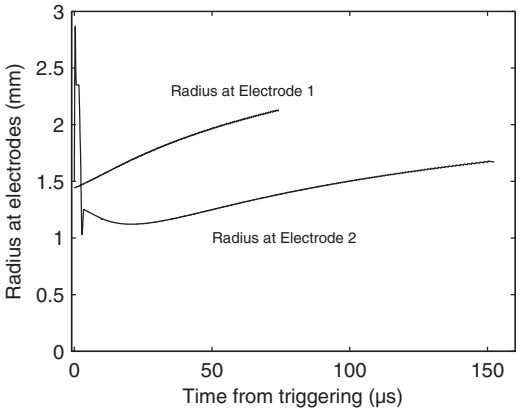

Fig. 6 The jet radius at electrodes 1 and 2 during its passage between the electrodes, calculated using the data in Fig. 3

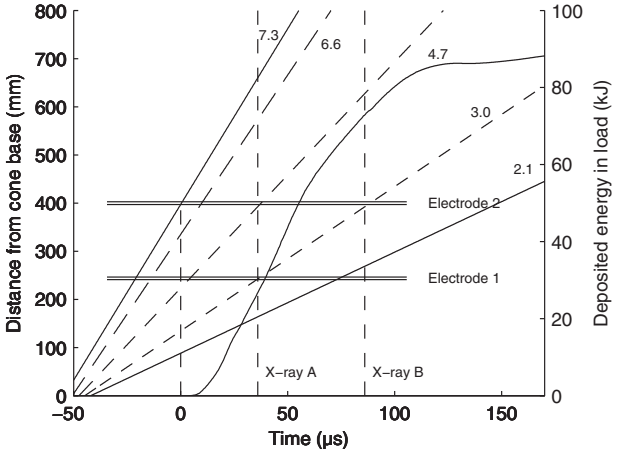

Fig. 8 Same position-time diagram as in Fig. 7 but with the deposited energy. Almost all energy has been deposited in the jet and electrode region by the time the rear part of the jet leaves the electrode region.

electrified and unelectrified jets since it is assumed that the electrification of the jet has no influence on the axial velocity of the jet. The diagonal lines marked by numbers indicate the paths of jet parts with the velocity given by the number (in km/s). The electrode positions are marked by horizontal lines. The parts of the jet with a velocity between 5.0 km/s and 7.3 km/s were between the electrodes at the time of triggering. The current pulse from the 96 kJ experiment is included in Fig. 7 and shows that the current pulse length is sufficiently long to affect a large portion of the jet. Figure 8 includes the estimated energy deposition as function of time. The energy stored in the PPS was 96 kJ and when the 2.1 km/s fragment leaves electrode 2 more than 87 kJ has been deposited in the jet or electrodes region. The mass of the portion of the jet with velocity higher than 2.1 km/s is 30.5 g according to Fig. 5, and hence the average specific energy deposition is 2.8 kJ/g. To heat copper with a temperature of 300 K to the boiling point requires about 1.3 kJ/g and about 6 kJ/g to vaporize it. Hence, in this example about 30% of the jet mass has been evaporated on average assuming that all of the energy is deposited in the jet. The load power is shown in Fig. 9, indicating a peak power of 1.5 GW. The part of the jet with a velocity between 7.3 km/s and 6.6 km/s has been subjected to a low power during its time between the electrodes compared with the rest of the jet and may explain the low radial velocity of this part of the jet [1], compare with Fig. 2.

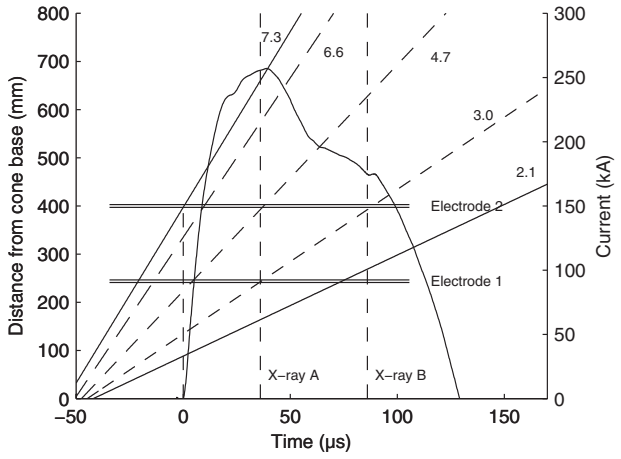

Fig. 7 Position-time diagram for the jet with the current pulse. The vertical dashed lines marked X-ray A and X-ray B marks the times (36 μs and 86 μs) when the X-ray pictures were taken. At time 36 μs, the part with velocity between 3 km/s and 4.7 km/s is between the electrodes and at time 86 μs, the part with velocity between 1.9 km/s and 3 km/s is between the electrodes.

3.3 Jet Resistance and Heating of the Jet. The jet resistance of the 39 kJ and 96 kJ experiments is shown in Fig. 10. The resistance in the 96 kJ experiment is between 20 mΩ and 25 mΩ throughout the pulse while in the 39 kJ experiment, the resistance is initially about the same as in the 96 kJ but increases to about 40 mΩ half way into the pulse. The measured resistances include both that of the jet and the contact points at the electrodes. The heating and resistance increase of electrically exploded metal conductors is most complex once the wire has melted and begun to disintegrate. To investigate the validity of simple heating models, the heating and resistance of the jet is calculated using the measured current passing through it and the estimated jet flow between the electrodes. For such a calculation, the current action integral method is used. By dividing the jet into small segments and calculate the current action integral [3] for each segment the time it is in between the electrodes, a temperature profile along the jet can be obtained. At given values of the action integral, the temperature reaches the melting and the vaporization temperatures. The resistance of the cylinder increases as a function of the

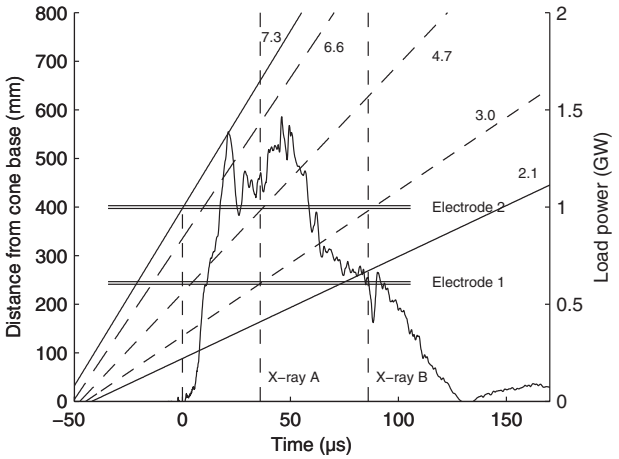

Fig. 9 Same position-time diagram as in Fig. 7 but with the power deposition in the jet. Note the low power up to the time the 6.6 km/s fragment leaves the electrode region, which may explain the low radial dispersion velocity of the tip.

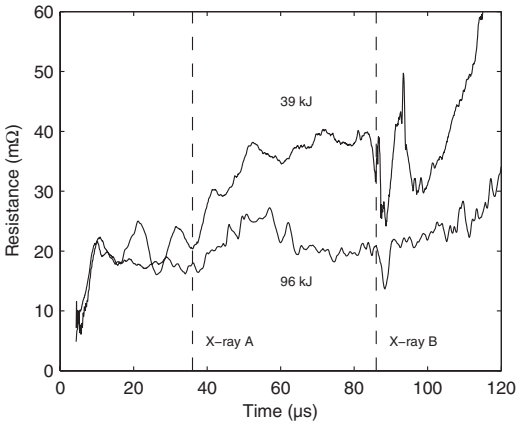

Fig. 10 The measured resistance of the jets in the 39 kJ and 96 kJ experiments

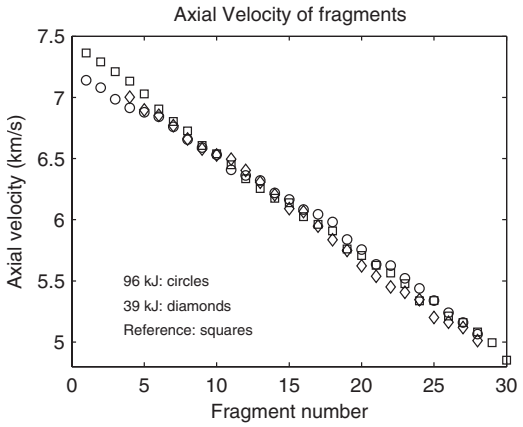

Fig. 12 The axial velocity for individual fragments in the 39 kJ (diamonds), 96 kJ (circles), and for an unelectrified jet (squares). The axial velocity as function of fragment number is similar for the electrified and unelectrified jets and this shows that electrified jets break up into the same number of fragments and with similar velocity distribution as the unelectrified jet.

action integral and take into account the different phases and transformations. In this analysis, the action integral values for copper obtained by Tucker and Toth [3] is used. The jet is assumed to have an initial temperature of 1000 K, reducing the required current action integral values to reach melting and the vaporization temperatures. It is assumed that the current flows homogeneously through a jet segment as soon as it enters the electrode region and disappear as soon as it leaves the electrode region. The current in the 96 kJ experiment is used as input in the calculation. The calculated resistance of the part of the jet that is between the electrodes is shown in Fig. 11 together with the energy deposition. The peak resistance value is 4.4 mΩ and drops of as the radius of the segments entering the electrode region increases, as shown in Fig. 6. The resistance value is a factor 5 lower compared with the experimental data, Fig. 10, and results in a much lower energy deposition.

3.4 Instability Growth. A shaped-charge jet naturally breaks up into fragments due to inherent instabilities of the jet itself. When an electric current passes through a jet, compressive magnetic forces will act on the jet and then enhance the natural radial variations and accelerate the break up of the jet. Figure 12 shows the axial velocity versus fragment number for the 39 kJ and 96 kJ experiment together with data for nonelectrified jet. The axial velocity as function of fragment number is similar for the electrified and unelectrified jets and this shows that electrified jets break up into the same number of fragments and with similar velocity distribution as the unelectrified jet. This indicates that the current interaction indeed enhances natural fragmentation. The velocity difference between two adjacent fragments is about 90 m/s on average, although with a large spread (standard deviation of 30 m/s). The velocity distribution of the jet, see Fig. 3, is used to find the approximate number of incipient fragments that is between the electrodes at times 36 μs and 86 μs by dividing the jet, excluding the tip fragment, into parts with a velocity difference of 90 m/s. At time 36 μs about 19 incipient fragments is between electrodes, while at time 86 μs, the corresponding number is about 12. The lengths of these incipient fragments or, in other words, the distance between two neighboring necks of the part between the electrodes is about 8 mm at time 36 μs, whereas at time 86 μs, it is about 12 mm. Figure 13 shows the X-ray picture of parts of the jet that is between the electrodes in experiments at time 31 μs with energy 0 kJ and at time 36 μs for energies 39 kJ and 96 kJ. With the aid of the position-time diagram in Fig. 7, it can be seen that at time 36 μs, the part with axial velocity 4.7 km/s is about to exit and the part with axial velocity 3.0 km/s has just entered the electrode region. Figure 14

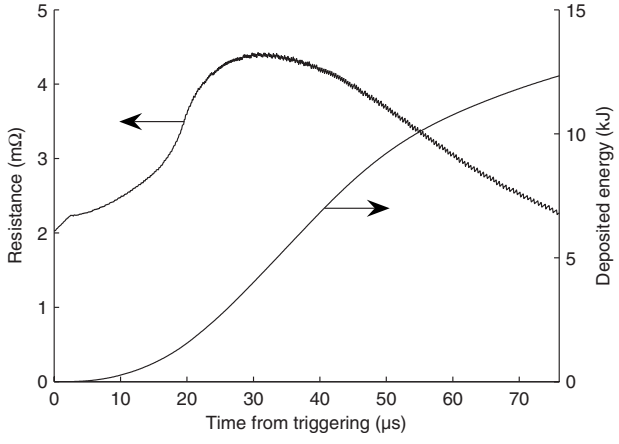

Fig. 11 The calculated resistance of the part of the jet that is between the electrodes and the energy deposited in the jet. The rise in resistance in the first 20 μs is due to heating. The resistance then drops due to the larger conducting area of the jet parts entering the electrode region and also due to decreasing current. The energy deposition is much lower than measured in the experiments.

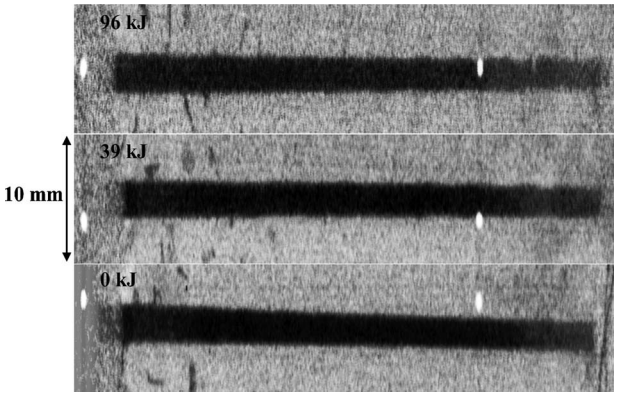

Fig. 13 The jet between the electrodes in experiments with energies of 0 kJ, 39 kJ, and 96 kJ stored in the capacitors. The 0 kJ experiment is depicted at time 31 μs and the 39 kJ and 96 kJ experiments are depicted at time 36 μs. The jet radius is scaled ×3. The white spots are markers for measurements.

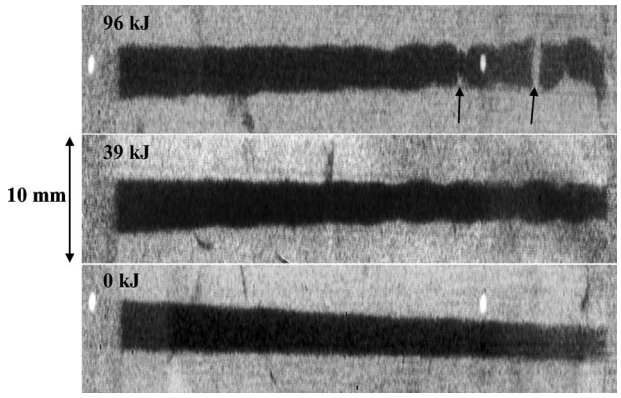

Fig. 14 The jet between the electrodes in experiments with energies of 0 kJ, 39 kJ, and 96 kJ stored in the capacitors. The 0 kJ experiment is depicted at time 81 μs and the 39 kJ and 96 kJ experiments are depicted at time 86 μs. The jet radius is scaled ×3. In the 96 kJ experiment, the jet has begun to disintegrate, indicated by the arrows. The white spots are markers for measurements.

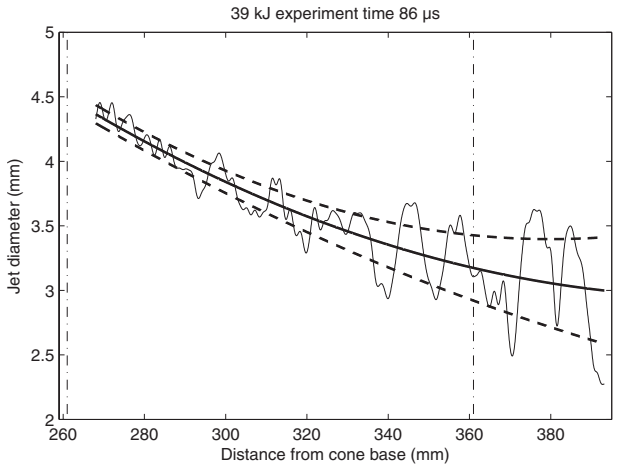

Fig. 15 The jet diameter along the jet in the 39 kJ experiments at 86 μs, extracted from Fig. 14. The solid, fat line is a second-order polynomial fitted to the diameter to obtain the mean diameter of the jet and the dashed lines are the mean diameter plus and minus the deviation shown in Fig. 16. The vertical dash-dotted lines mark the position of the white reference markers in Fig. 14.

shows corresponding situation at times 81 μs (0 kJ) and 86 μs (39 kJ and 96 kJ). The part with axial velocity 3.0 km/s is about to exit and the part with axial velocity 1.9 km/s has just entered the electrode region at time 86 μs. Note however that the X-ray pictures do not view all of the jet due to shadows from the electrodes. The white spots in the X-ray pictures are markers for measurements. Although the jet has been subjected to a relatively high current, the radial variation is barely visible at time 31/36 μs. At time 86 μs, the radial variation is strong in the electrified jets and in the 96 kJ experiment, the jet is broken at two places (black arrows).

The X-ray pictures were digitally processed and the jet diameter along the jet was extracted. A second-order polynomial

$$d(z) = A(z - z_0)^2 + B(z - z_0) + C \tag{1}$$

was fitted to the extracted diameter to obtain a mean diameter along the jet, where z is the position along the jet between the electrodes and z_0 is about 0.27 m from the cone base. In order to quantify the instability growth, another second-order polynomial

$$\Delta d(z) = D(z - z_0)^2 + E(z - z_0) + F \tag{2}$$

is fitted to the absolute value of the difference between the extracted diameter and the average diameter. This gives an estimate of the deviation δ from the average diameter. Figure 15 shows the extracted diameter along the jet for the 39 kJ experiments at time 86 μs, together with the mean diameter $d(z)$, solid line, and the mean diameter plus and minus the deviation $d(z) \pm \Delta d(z)$, dashed lines. The vertical dash-dotted lines correspond to the position of the white markers in Fig. 14. Figure 16 shows the difference between the extracted diameter and the mean diameter, together with the mean deviation for the 39 kJ experiment at time 86 μs. Figure 17 shows the same traces for the unelectrified jet at time 81 μs. The deviation from the mean diameter indicates no significant growth of the instabilities and provides a reference for the "natural" deviation of about 0.1 mm on average. The values of the constants in the fitted polynomials are given in Table 2. The 0 kJ experiment is depicted 5 μs earlier than the 39 kJ and 86 kJ experiments, during which the jet moves between 10 mm and 15 mm but has a small effect on the jet diameter. Figures 18 and 19 shows the mean diameter and the deviation for all three experiments at times 31/36 μs and 81/86 μs. At time 31/36 μs, the deviation is not significantly different but at 81/86 μs, the deviation is significantly larger for the electrified jets. The calculated diameter, using the radius and velocity distribution of Fig. 3, is included in the graphs (fat solid line). A growth velocity of the deviation can be estimated using the velocity distribution along the jet. The average growth velocity G of the deviation δ for a point i on the jet is calculated for the 86 μs case in the 39 kJ experiment using

$$G_i = \frac{\Delta\delta}{\Delta t} = \frac{\delta_i - \delta_{\min}}{\dfrac{z_i - z_{\min}}{v_i}} \tag{3}$$

where $\delta_{\min}$ is the minimum deviation at the axial position $z_{\min}$ (marked by the circle in Fig. 19) and v_i is the velocity of the point i. Figure 20 shows the growth velocity of the deviation along part of the jet (the part between the circle and the square in Fig. 19) together with the axial velocity of the jet for the 39 kJ experiment at time 86 μs. The growth rate increases along the jet and reaches a velocity of the order of 10 m/s and the acceleration is thus of the order of 10^5 m/s^2.

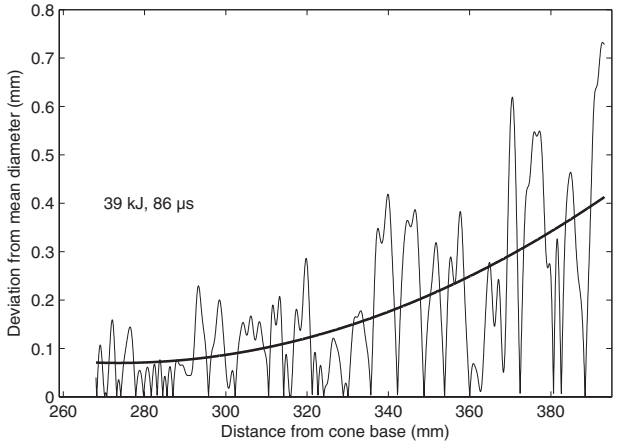

Fig. 16 The deviation from the mean diameter of the jet in the 39 kJ experiments at 86 μs. The solid, fat line is the second-order polynomial fitted to the deviation from the mean diameter and indicates a clear growth of the instability from 0.07 mm to 0.5 mm.

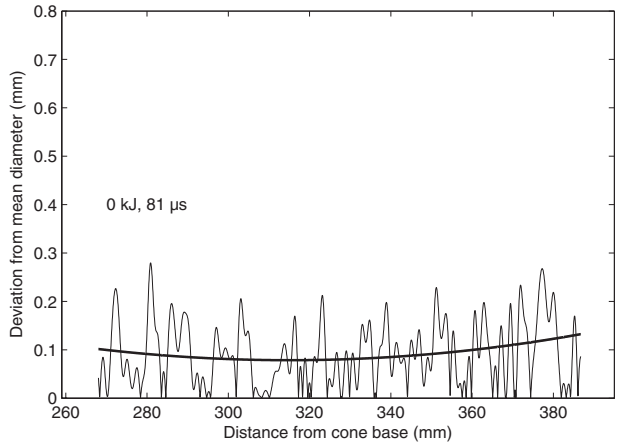

Fig. 17 The deviation from the mean diameter of the jet in the 0 kJ experiments at 81 μs. The solid, fat line is the second-order polynomial fitted to the deviation from the mean diameter and indicates no growth of the instability and provides a reference for the natural deviation. Note that this reference level is around 0.1 mm all along the jet while in the 39 kJ experiment, the deviation grows from approximately this value. Note that the 0 kJ experiment is depicted at 5 μs earlier than the 39 kJ experiment in which the jet moves between 10 mm and 15 mm.

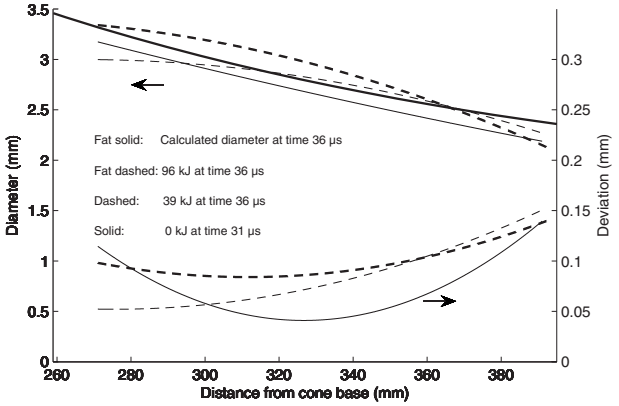

Fig. 18 Plot of the mean diameter along the jets at time 31/36 μs for the 0 kJ, 39 kJ, and 96 kJ experiments together with the diameter deviation from the mean diameter. At this time, the deviations are not significantly different and a normal deviation is about 0.1 mm.

4 Discussion

In the 96 kJ experiment, the average energy deposition in the jet was 2.8 kJ/g, which is sufficient to bring the jet to the boiling point and evaporate about one third of the jet. This assumes that losses are small in the contact between the jet and electrodes and that no current paths parallel to the jet exists. An attempt was made to calculate the energy deposition and jet resistance using the jet flow information and the experimental current but yielded about five times lower energy deposition and jet resistance than observed in the experiments. The heating of the jet is a complex process and, as was found by Taylor [4–6] and Appelgren et al. [7] in experiments with electrically exploded copper conductors, the resistance was significantly higher than could be attributed to simple heating. To explain the high resistance measured in his exploding wires experiments, Taylor suggested the existence of an electrically insulating boundary layer around condensed fragments of the wire. Other possible explanations include the fact that the calculation does not include resistive losses in the electrodes or in the contact between the electrodes and the jet. Neglecting the finite magnetic field diffusion time may also be a source of error, but calculations using a 2D hydrocode [8] indicate that the current flows relatively homogeneously soon after reaching the flat top of the pulse and that the temperature does not vary significantly in the radial direction. There is also the possibility that the current path is longer than what is given by the electrode distance, i.e., the current path is dragged out of the electrode region and the return path of the current to the electrode is provided by an arc. The higher resistance in the 39 kJ experiment compared with the 96 kJ experiment for part of the pulse may be explained by a longer current path. Another possible source of losses, not taken into account in the modeling, is the mechanisms associated with the radial acceleration of jet material. The energy for this radial expansion of the jet must come from the electric heating of the jet.

There are several mechanisms suggested for the disruption of jets that interacts with a current pulse. The effect of the magnetohydrodynamic instabilities on stretching metal jets was investigated analytically by Littlefield using perturbation analysis [9–11]. His conclusion was that the current significantly increases the instabilities and reduces the time for break up of the jet into fragments. By analyzing the radiographs of the jet between the electrodes in our experiments it could be concluded that the current indeed enhances the natural fragmentation of the jet and that the fragmentation increases for higher amount of deposited electric energy. Analysis of the radiographs also shows that the rate at which the jet neck diameter is reduced is of the order of 10 m/s.

It has been suggested that the magnetic forces compressing the necks are responsible for the formation of the disks that are observed some time after the electrification [12]. The disks would, according to the suggested model, be formed by jet material that is forced away from the neck into the large diameter part fragments, eventually forming the thin disks, and numerical calculations show that this type of material flow is possible [13]. However, in the experiments by Appelgren et al. [1], the velocity of the expanding rings is of the order of 100 m/s, i.e., one order of magnitude faster than the growth rate of the instabilities. In the radiographs of the electrode region in the 96 kJ experiment, the jet is observed to break up, implying an electrical explosion. Electrical explosions of conductors can eject material at a velocity of several hundred m/s [7]. Hence, the disruption mechanism in these ex-

Table 2 Values of the constants in the Eqs. (1) and (2)

Experiment (kJ)	Values of the constants of the polynomials					
	A ($\times 10^{-6}$)	B ($\times 10^{-3}$)	C	D ($\times 10^{-6}$)	E ($\times 10^{-3}$)	F
0 at 31 μs	9.72	−9.38	3.17	23.8	−2.64	0.115
39 at 36 μs	−46.8	−0.461	3.00	7.36	−0.0641	0.0522
96 at 36 μs	−53.1	−3.56	3.34	8.56	−0.695	0.0981
0 at 81 μs	−10.6	−11.4	4.29	10.5	−0.983	0.102
39 at 86 μs	59.0	−18.3	4.36	24.0	−0.266	0.0708
96 at 86 μs	−53.1	−3.56	3.34	40.6	−1.66	0.122

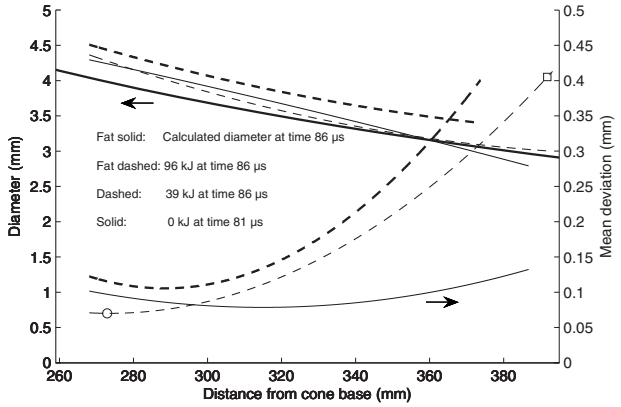

Fig. 19 Plot of the mean diameter along the jets at time 81/86 μs for the 0 kJ, 39 kJ, and 96 kJ experiments together with the diameter deviation from the mean diameter. At this time, the effect of electric energy on deviations is strong. The circle and the square marks the interval of the jet used to calculated the growth velocity in Fig. 20.

periments is thought to be a combination of instability growth due to magnetic forces and electrical explosions due to ohmic heating. These two effects reinforce each other as the magnetic forces acting in the necks reduce the conducting area and enhance the energy deposition. The heated material looses strength and can be reduced further until the current density and temperature result in an electrical explosion of the neck. Similar conclusions were reported by Mayseless et al. [14] who performed experiments on and numerical simulations of exploding rods with necks.

The suggested mechanism is based on a few experiments with one type of shaped-charge device and with a single experimental setup and should be supported by more experiments with other experimental settings and jet characteristics.

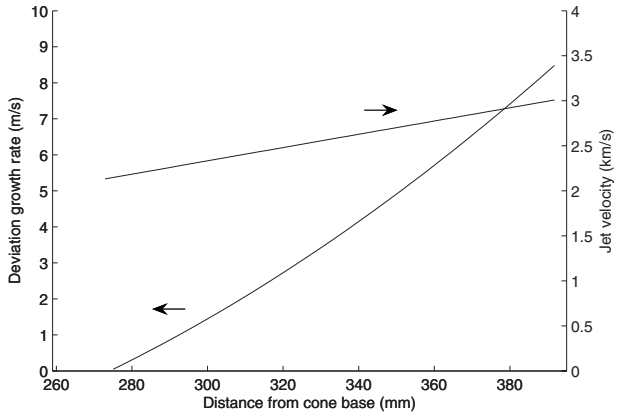

Fig. 20 Plot of the deviation growth velocity along the jet at time 86 μs for the 39 kJ experiments together with the jet velocity. The velocity reaches about 10 m/s toward the end of the interaction, indicating an acceleration of the order of 10^5 m/s^2.

5 Conclusions

The interaction between a solid copper jet and electrical current pulse as the jet passes between two electrodes was studied. The shape of, and the velocity distributions along, the jet has been used to estimate the correlation between the jet mass flow through the electrodes and the electrical energy deposition. On average, 2.8 kJ/g was deposited in the jet and electrode region, which is sufficient to bring the jet up to the boiling point but not to the point of vaporization. A model based on the assumption of a homogenous current flow through the jet between the electrodes underestimates the energy deposition and the jet resistance by a factor 5 compared with the experiments, indicating a more complex current flow through the jet.

The experimental results indicate the following mechanism for the enhancement of jet breakup. When electrified, the natural-formed necks in the jet are subjected to a higher current density compared with other parts of the jet. The higher current density results in a stronger heating and a stronger magnetic pinch force. Eventually, the jet material in the neck is evaporated and explodes electrically, resulting in a radial ejection of vaporized jet material.

References

[1] Appelgren, P., Skoglund, M., Lundberg, P., Westerling, L., Larsson, A., and Hurtig, T., 2010, "Experimental Study of Electromagnetic Effects on Solid Copper Jets," J. Appl. Mech., **77**(1), p. 011010.

[2] Senior, P., Smith, I. R., Appelgren, P., Elfsberg, M., Lundberg, P., and Skoglund, M., 2006, "A 400 kJ Mobile Pulsed Power System With Variable Pulse Forming," *Proceedings of the MegaGauss XI*, London, UK, pp. 257–261.

[3] Tucker, T. J., and Toth, R. P., 1975, "EBW1: A Computer Code for the Prediction of the Behavior of Electrical Circuits Containing Exploding Wire Elements," Sandia Laboratories Report No. SAND-75-0041.

[4] Taylor, M. J., and Dunnet, J., 2003, "A Description of the Wire Explosion Process for ETC Plasma Generators," IEEE Trans. Magn., **39**(1), pp. 269–274.

[5] Taylor, M. J., 2002, "Formation of Plasma Around Wire Fragments Created by Electrically Exploded Copper Wire," J. Phys. D: Appl. Phys., **35**, pp. 700–709.

[6] Taylor, M. J., 2002, "Plasma Propellant Interactions in an Electrothermal-Chemical Gun," Ph.D. thesis, Cranfield University, Swindon, UK.

[7] Appelgren, P., Larsson, A., Lundberg, P., Skoglund, M., and Westerling, L., 2009, "Studies of Electrically-Exploded Conductors for Electric Armour Applications," Acta Phys. Pol. A, **115**(6), pp. 1072–1074.

[8] Appelgren, P., Westerling, L., Skoglund, M., Lundberg, P., Hurtig, T., and Larsson, A., 2008, "Radial Jet Dispersion Due to Current Interaction in an Electric Armor Application," 24th International Symposium on Ballistics, New Orleans, LA, Sept. 22–26.

[9] Littlefield, D. L., and Powell, J. D., 1990, "The Effect of Electromagnetic Fields on the Stability of a Uniformly Elongating Plastic Jet," Phys. Fluids A, **2**(12), pp. 2240–2248.

[10] Littlefield, D. L., 1991, "Finite Conductivity Effects on the MHD Instabilities in Uniformly Elongating Plastic Jets," Phys. Fluids A, **3**(6), pp. 1666–1673.

[11] Littlefield, D. L., 1994, "Thermomechanical and Magnetohydrodynamic Stability of Elongating Plastic Jets," Phys. Fluids, **6**(8), pp. 2722–2729.

[12] Shvetsov, G. A., 1999, "Disruption of Shaped Charge Jets Due to Axial Current," 18th International Symposium on Ballistics, San Antonio, TX, Nov. 15–19.

[13] Robertson, I., Clegg, R., Burton, A., Hayhurst, C., Riley, C., Simkin, J., Moor, E., Ratcliff, P., and Cliffe, R., 2004, "Insights From Numerical Modeling of Electric Armor Using Hydrocode and Electromagnetic Software," *Proceedings of the 12th Electromagnetic Launch Technology Symposium*, Snowbird, UT, May 25–28.

[14] Mayseless, M., Gruss, E., Me-Bar, Y., Surujon, Z., and Rosenberg, A., 2004, "Electrical Explosion of Undulated Wires," *Proceedings of the 21st International Symposium on Ballistics*, Adelaide, South Australia, Apr. 19–23, pp. 324–330.